Wave-equation extended images for semblance and depth focusing velocity analysis

Tongning Yang and Paul Sava, Center for Wave Phenomena, Colorado School of Mines*

SUMMARY

Conventional velocity analysis applied to images produced by wave-equation migration makes use either of moveout information from space-lags, or of focusing information from time-lags. However, more robust velocity estimation methods can be designed to take advantage at the same time of the moveout and focusing information provided by the migrated images. Such joint velocity estimation requires characterization of the analytic moveout surface defined for space-lag and time-lag common-image gathers. The analytic expressions for such surfaces are nonlinear, but reduce naturally to the conventional space-lag (linear) and time-lag (nonlinear) moveout functions. A joint migration velocity analysis technique exploiting the entire extended imaging condition information has the potential to benefit from the robustness of depth focusing analysis and of the high resolution of conventional semblance analysis.

INTRODUCTION

A key challenge for imaging in complex geology is an accurate determination of a velocity model in the area under investigation. Migration velocity analysis is based on the principle that image accuracy indicators are optimized when data are correctly imaged. A common procedure for velocity analysis is to examine the alignment of images created with multi-offset data. An optimal choice for image analysis in complex areas is the angle domain which is free of complicated artifacts present in surface offset gathers (Stolk and Symes, 2004). If images constructed by illuminating a point from various directions are aligned, then the velocity model used for imaging is accurate. This idea is usually referred to as the *semblance principle* (Yilmaz, 2001) and it represents the foundation of most velocity analysis methods in use today.

Several methods have been proposed for angle decomposition (Sava and Fomel, 2003b,a; Fomel, 2004; Biondi and Symes, 2004). All these procedures require decomposition of extrapolated wavefields or of migrated images in components that are related to the reflection angles. Here, we emphasize a special angle decomposition method which exploits properties of migrated images. This imaging procedure requires the application of an *extended imaging condition* (Sava and Fomel, 2006; Sava, 2007) which implements a point-by-point comparison of the source and receiver wavefields extrapolated from the surface. In general, the comparison is done using simple image processing procedures applied at every location in the subsurface. If the source and receiver wavefields match each-other, then their cross-correlation maximizes at zero lag in space and time; otherwise, their cross-correlation does not maximize at zero lag indicating wavefield reconstruction, e.g. due to velocity inaccuracy. Thus, a straightforward way of approaching migration velocity analysis is to exploit the image information from non-zero lags.

The source and receiver wavefields used for imaging are 4D objects, function of space coordinates and time (or frequency). For simplicity, we discuss in this paper only time-domain imaging, although our analysis applies equally well for frequency domain imaging. For such 4D objects, the images obtained by extended imaging conditions are characterized in general by a 3D space-lag vector and a 1D time-lag. The images constructed with space and time-lags can be decomposed function of reflection angles using the geometric relations between incident and reflected rays (Sava and Fomel, 2006).

Conventional migration velocity analysis exploits separately either space-lag information, by *semblance analysis* (Sava and Biondi, 2004a,b; Biondi and Symes, 2004), or the time-lag information, by *depth focusing analysis* (Faye and Jeannot, 1986; MacKay and Abma, 1992, 1993; Nemeth, 1995, 1996; Sava and Fomel, 2006). However, we suggest here that a more robust velocity analysis approach combines the information provided by the space and time-lags and optimize migrated images using all available information. This way, we can leverage at the same time the robustness of depth focusing analysis and the high resolution of semblance analysis.

In this paper, we analyze the moveout function for common-image gathers constructed by extended imaging conditions applied after conventional wavefield extrapolation. We derive the analytic expression of the moveout function for space and time-lag extended imaging conditions and compare it with the better known special cases of imaging with space and time-lags separately. This analysis represents a prerequisite for velocity estimation based on the departure of migrated images from a reference corresponding to imaging with accurate velocity.

WAVE-EQUATION IMAGING CONDITIONS

Under the single scattering approximation, seismic migration consists of wavefield reconstruction and an imaging condition. Wavefield reconstruction forms solutions to a wave-equation with recorded data as boundary condition. We can consider many different numeric solutions to the acoustic wave-equation, but regardless of the specific implementation, we reconstruct one wavefield by forward time propagation from the source and one wavefield by backward time propagation from the receivers. Those source and receiver wavefields can be represented as four-dimensional objects function of position in space $\mathbf{x} = (x, y, z)$ and time t,

$$u_s = u_s(\mathbf{x}, t) \ , \tag{1}$$

$$u_r = u_r(\mathbf{x}, t) \ . \tag{2}$$

The imaging condition is designed to extract from these extrapolated wavefields the locations where reflectors occur in the

subsurface. The image $r\,(\mathbf{x})$ is obtained from the reconstructed wavefields by evaluating the match between them at every location in the subsurface. A conventional imaging condition (Claerbout, 1985) forms an image as the zero cross-correlation lag between the source and receiver wavefields:

$$r\,(\mathbf{x}) = \int u_s\,(\mathbf{x},t)\,u_r\,(\mathbf{x},t)\,dt\;. \tag{3}$$

An alternative (extended) imaging condition (Rickett and Sava, 2002; Sava and Fomel, 2006), also evaluates the match between the source and receiver wavefields by their cross-correlation, but it preserves the space and time-lags:

$$r\,(\mathbf{x},\boldsymbol{\lambda},\tau) = \int u_s\,(\mathbf{x}-\boldsymbol{\lambda},t-\tau)\,u_r\,(\mathbf{x}+\boldsymbol{\lambda},t+\tau)\,dt\;. \tag{4}$$

The quantities $\boldsymbol{\lambda}$ and τ represent the spatial and temporal cross-correlation lags between the source and receiver wavefields. If the local cross-correlation between them maximizes at zero lag on all four dimensions, then those wavefields are extrapolated correctly, i.e. form an image. If this is not the case, then we can conclude that the wavefield reconstruction is incorrect, indicating incorrect velocity or incorrect wavefield extrapolation or irregular illumination, etc.

SPACE- AND TIME-LAG MOVEOUT ANALYSIS

For the purpose of migration velocity analysis, it is necessary to understand the correct moveout shape of the images formed using extended imaging conditions. In particular, we would like to specify the shape of the moveout curves corresponding to common-image gathers (CIG), i.e. the function $z = z\,(\boldsymbol{\lambda},\tau)$, in order to analyze if the images are correctly formed in the subsurface.

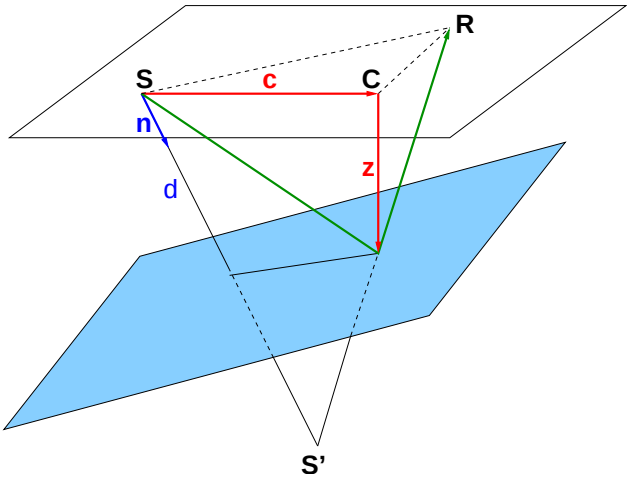

Figure 1: Geometry of reflection a experiment. **S**, **R** and **C** identify the positions of the source, receiver and image, respectively. The reflector is located at distance d from the source position in the direction of the vector **n**. The position of the CIG relative to the source is indicated by the vectors **c** and **z**.

Consider the reflection geometry depicted in Figure 1: the unit vector $\mathbf{n} = \{n_x, n_y, n_z\}$ and the distance d identify the position of the reflection plane; the vector $\mathbf{c} = \{c_x, c_y\}$ identifies the fixed horizontal position of a CIG relative to the source position. We consider the case when extended imaging conditions are computed function of horizontal space-lags $\boldsymbol{\lambda} = \{\lambda_x, \lambda_y, 0\}$ and time-lag τ. Although we consider here only horizontal space-lags, the same logic applies to the more general case when the space $\boldsymbol{\lambda}$ is three-dimensional. Using those definitions, the coordinates of the reflection point $\{c_x, c_y, z\}$ can be found at the intersection of idealized incident (source) and reflected (receiver) wavefields, i.e. by solving the system:

$$\|\mathbf{c}+\mathbf{z}\| = v t\;, \tag{5}$$

$$\|\mathbf{c}+\mathbf{z}-2\mathbf{n}d\| = v t\;, \tag{6}$$

where $\mathbf{z} = \{0, 0, z\}$ with z representing the depth of the reflection point.

Solving this system for the image depth z at coordinates $\{c_x, c_y\}$ corresponds to the application of the conventional imaging condition 3. Likewise, we can simulate the application of the extended imaging condition 4 by solving the system

$$\|\mathbf{c}+\mathbf{z}+\boldsymbol{\lambda}\| = v\,(t+\tau) \tag{7}$$

$$\|\mathbf{c}+\mathbf{z}-2\mathbf{n}d-\boldsymbol{\lambda}\| = v\,(t-\tau)\;, \tag{8}$$

where the two surfaces representing the idealized source and receiver wavefields are shifted in space by the quantity $\boldsymbol{\lambda} = \{\lambda_x, \lambda_y, 0\}$ and in time by the quantity τ. In other words, we can define the problem as solving for the magnitude of the vector **z** function of variables $\boldsymbol{\lambda}$ and τ at fixed CIG coordinates $\mathbf{c} = \{c_x, c_y, 0\}$.

A formal solution to the system 7-8 leads to the following expression for the reflector depth z at the CIG coordinates $\{c_x, c_y\}$:

$$z\,(\boldsymbol{\lambda},\tau) = (n_z d)\,K + v\tau\sqrt{K^2 + \frac{\|\mathbf{c}+\boldsymbol{\lambda}\|^2}{(n_z d)^2 - (v\tau)^2}}\;, \tag{9}$$

where quantity K is defined by

$$K = 1 - \frac{(\mathbf{c}\cdot\mathbf{n})\,d - \left(n_x^2+n_y^2\right) + (\mathbf{c}+\mathbf{n}d)\cdot\boldsymbol{\lambda}}{(n_z d)^2 - (v\tau)^2}\;. \tag{10}$$

Figure 2 depicts the reflection moveout curve defined by equations 9-10 for the case of normal incidence on a horizontal reflector, i.e. $\mathbf{n} = \{0, 0, 1\}$. This surface has a complex shape which is not immediately intuitive. However, it is easier to analyze this surface using better studied special cases:

Space-lag moveout: For the case when we construct CIGs function of space-lags only, i.e. $\tau = 0$, the moveout surface 9 reduces to the form

$$z\,(\boldsymbol{\lambda}) = (n_z d)\,K_{\boldsymbol{\lambda}}\;, \tag{11}$$

where

$$K_{\boldsymbol{\lambda}} = 1 - \frac{(\mathbf{c}\cdot\mathbf{n})\,d - \left(n_x^2+n_y^2\right) + (\mathbf{c}+\mathbf{n}d)\cdot\boldsymbol{\lambda}}{(n_z d)^2}\;. \tag{12}$$

This special case shows a linear dependence of depth with horizontal space-lags, with a coefficient which depends on the reflection angles on the reflector, thus justifying the angle decomposition methods based on slant-stacks applied to space-lag CIGs (Sava and Fomel, 2003a; Biondi and Symes, 2004;

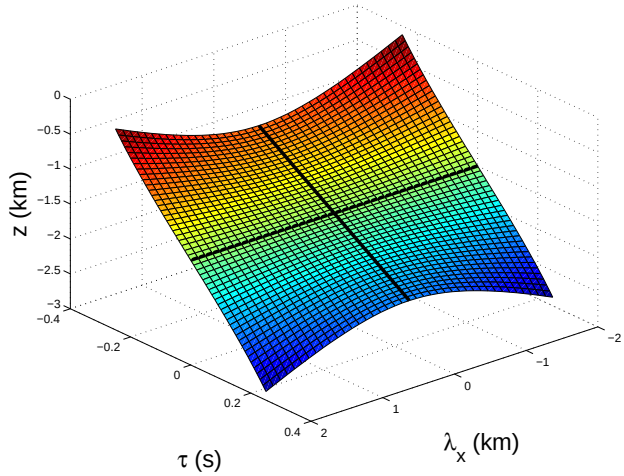

Figure 2: Moveout surface $z = z(\lambda_x, \tau)$ according to equations 9 and 10 for a horizontal reflector.

Fomel, 2004). This linear relation is even more obvious for the case of a horizontal reflector, $\mathbf{n} = \{0, 0, 1\}$, when equations 11-12 reduce to

$$z(\lambda_x, \lambda_y) = d - \frac{c_x \lambda_x + c_y \lambda_y}{d} \ . \tag{13}$$

In this situation, d represents the reflector depth.

Time-lag moveout: For the case when we construct CIGs function of time-lags only, i.e. $\boldsymbol{\lambda} = 0$, the moveout surface 9 reduces to the form

$$z(\tau) = (n_z d) K_\tau + v\tau \sqrt{K_\tau^2 + \frac{\|\mathbf{c}\|^2}{(n_z d)^2 - (v\tau)^2}} \ , \tag{14}$$

where

$$K_\tau = 1 - \frac{(\mathbf{c} \cdot \mathbf{n})\, d - \left(n_x^2 + n_y^2\right)}{(n_z d)^2 - (v\tau)^2} \ . \tag{15}$$

This special case shows a nonlinear dependence of depth with time-lag. This nonlinear relation is even more obvious for the case of a horizontal reflector, $\mathbf{n} = \{0, 0, 1\}$, when equations 14-15 reduce to

$$z(\lambda_x, \lambda_y) = d + v\tau \sqrt{1 + \frac{\|\mathbf{c}\|^2}{d^2 - (v\tau)^2}} \ . \tag{16}$$

In this situation, d represents the reflector depth.

EXAMPLE

We illustrate the moveout expressions from the preceding sections with a simple synthetic model consisting of a reflector embedded in a constant velocity medium. The data and the image obtained by modeling and migration with wavefield extrapolation are presented in Figures 3(a) and 3(b), respectively.

Figures 4(a)-4(e) and Figures 4(f)-4(j) depict space-lag CIGs corresponding to different image locations with angles of incidence of 0° and 18°, respectively. From left to right, the panels correspond to $\tau = \{-0.150, -0.075, 0, +0.075, +0.150\}$ s.

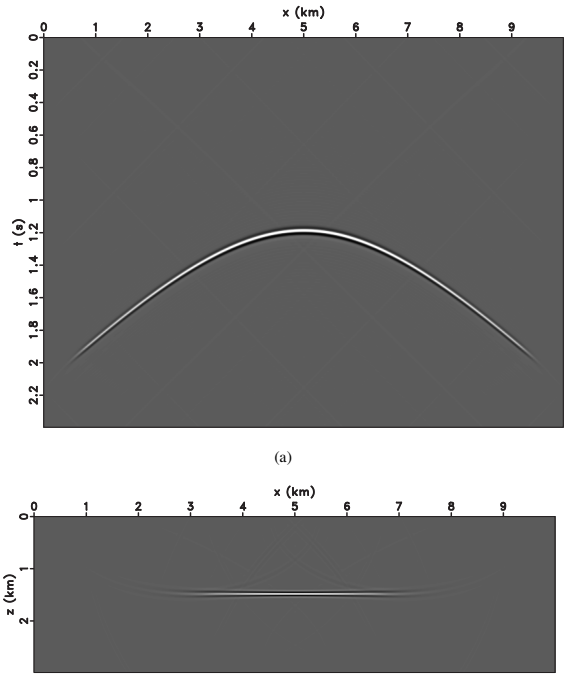

Figure 3: (a) Synthetic data and (b) migrated image.

The dashed line overlain on each panel corresponds to the function $z(\lambda_x)$ according to equation 9 at various values of τ. Similarly, Figures 5(a)-5(e) and Figures 5(f)-5(j) depict time-lag CIGs corresponding to the same image locations with angles of incidence of 0° and 18°, respectively. From left to right, the panels correspond to $\lambda_x = \{-0.8, -0.4, 0, +0.4, +0.8\}$ km. The dashed line overlain on each panel corresponds to the function $z(\tau)$ according to equation 9 at various values of λ_x. In both cases, the analytic formula derived in the preceding section accurately describes the moveout curves characterizing images obtained by wave-equation migration with extended imaging condition.

CONCLUSIONS

Extended imaging conditions offer the possibility to design robust migration velocity analysis techniques which exploit at the same time conventional semblance analysis and depth focusing analysis. The moveout functions characterizing the extended imaging conditions are non-planar analytic surfaces which reduce naturally to the conventional space-lag (linear) and time-lag (nonlinear) moveout functions. Extensions of this study concern the residual changes to the space-time moveout surface for inaccurate imaging velocity.

ACKNOWLEDGMENTS

We acknowledge the support of the sponsors of the Center for Wave Phenomena at Colorado School of Mines.

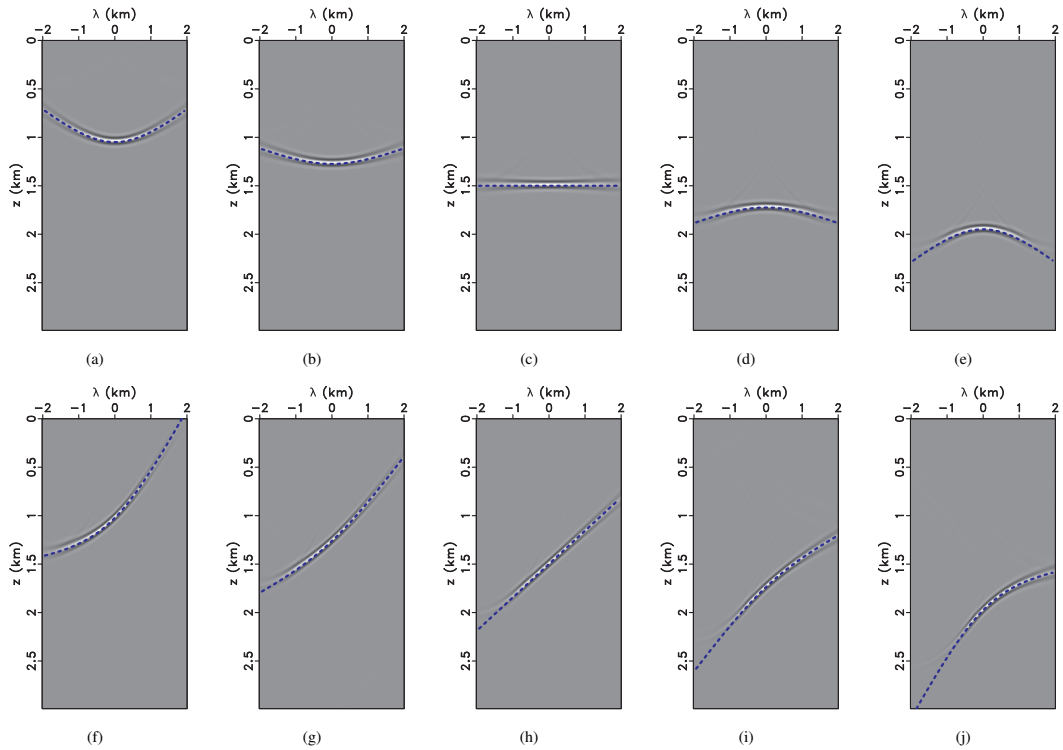

Figure 4: Space-lag CIGs for $\tau = \{-0.150, -0.075, 0, +0.075, +0.150\}$ s. Panels (a)-(e) and (f)-(j) correspond to angles of incidence of 0° and 18°, respectively.

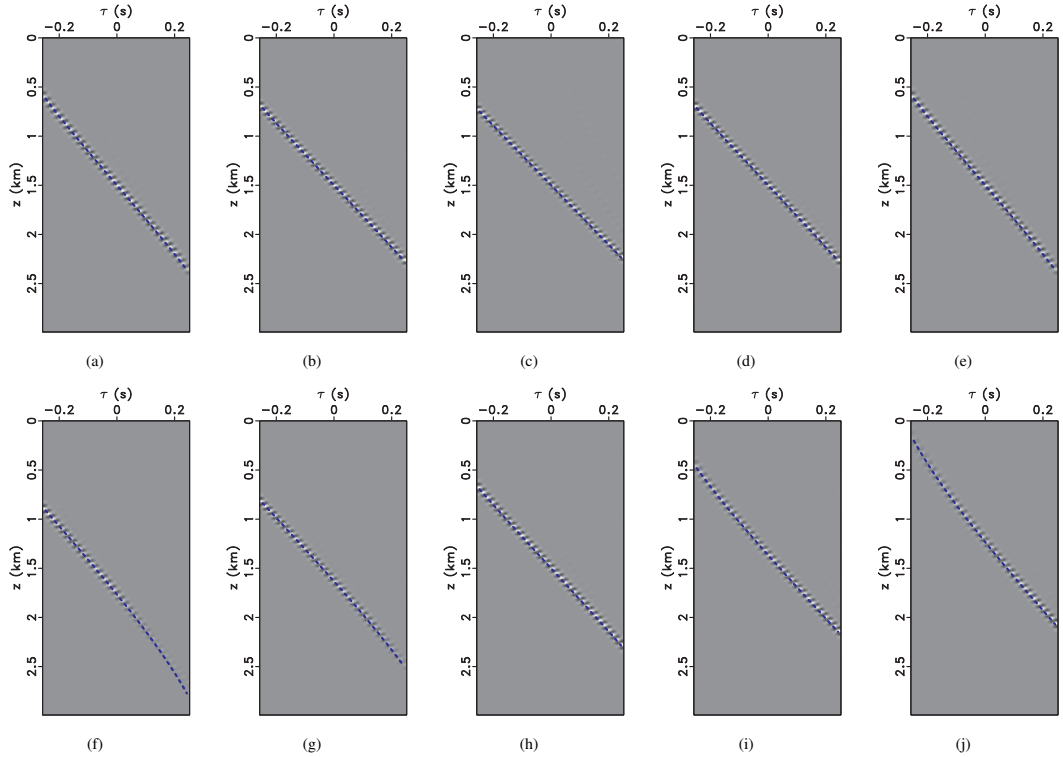

Figure 5: Time-lag CIGs for $\lambda_x = \{-0.8, -0.4, 0, +0.4, +0.8\}$ km. Panels (a)-(e) and (f)-(j) correspond to angles of incidence of 0° and 18°, respectively.

REFERENCES

Biondi, B. and W. Symes, 2004, Angle-domain common-image gathers for migration velocity analysis by wavefield-continuation imaging: Geophysics, **69**, 1283–1298.

Claerbout, J. F., 1985, Imaging the Earth's interior: Blackwell Scientific Publications.

Faye, J. P. and J. P. Jeannot, 1986, Prestack migration velocities from focusing depth analysis: 56th Ann. Internat. Mtg., Session:S7.6, Soc. of Expl. Geophys.

Fomel, S., 2004, Theory of 3-D angle gathers in wave-equation imaging: Presented at the 74th Annual International Meeting, SEG, Soc. of Expl. Geophys.

MacKay, S. and R. Abma, 1992, Imaging and velocity estimation with depth-focusing analysis: Geophysics, **57**, 1608–1622.

———, 1993, Depth-focusing analysis using a wavefront-curvature criterion: Geophysics, **58**, 1148–1156.

Nemeth, T., 1995, Velocity estimation using tomographic depth-focusing analysis: 65th Ann. Internat. Mtg, 465–468, Soc. of Expl. Geophys.

———, 1996, Relating depth-focusing analysis to migration velocity analysis: 66th Ann. Internat. Mtg, 463–466, Soc. of Expl. Geophys.

Rickett, J. and P. Sava, 2002, Offset and angle-domain common image-point gathers for shot-profile migration: Geophysics, **67**, 883–889.

Sava, P., 2007, Stereographic imaging condition for wave-equation migration: Geophysics (Letters), **72**, A87–A91.

Sava, P. and B. Biondi, 2004a, Wave-equation migration velocity analysis - I: Theory: Geophysical Prospecting, **52**, 593–606.

———, 2004b, Wave-equation migration velocity analysis - II: Subsalt imaging examples: Geophysical Prospecting, **52**, 607–623.

Sava, P. and S. Fomel, 2003a, Angle-domain common image gathers by wavefield continuation methods: Geophysics, **68**, 1065–1074.

———, 2006, Time-shift imaging condition in seismic migration: Geophysics, **71**, S209–S217.

Sava, P. C. and S. Fomel, 2003b, Angle-domain common-image gathers by wavefield continuation methods: Geophysics, **68**, 1065–1074.

Stolk, C. C. and W. W. Symes, 2004, Kinematic artifacts in prestack depth migration: Geophysics, **69**, 562–575.

Yilmaz, O., 2001, Seismic Data Analysis (2nd edition): Society of Exploration Geophysicists.